Supplemental Digital Content

Tidal recruitment assessed by Electrical Impedance Tomography and Computed Tomography in a porcine model of lung injury.

Thomas Muders, Henning Luepschen, Jörg Zinserling, Susanne Greschus, Rolf Fimmers, Ulf Guenther, Miriam Buchwald, Daniel Grigutsch, Steffen Leonhardt, Christian Putensen, Hermann Wrigge

Content

SDC-1 EIT data acquisition and processing

EIT images were recorded during one low flow breath (slow inflation) with a tidal volume of 12 ml/kg BW (350 - 420 ml) immediately after the CT scans. The EIT device (EIT evaluation kit 2, Dräger medical AG & Co. KG, Germany) produced image vectors $\Delta\mathbf{z}(t_k)$ with 912 elements (or pixels) each at discrete points in time t_k as described in [4]. In order to obtain the best temporal resolution, we set the maximal frame rate to 20 images per second so that $t_k - t_{k-1} = 50\text{ms}$. These image vectors show the impedance change at time t_k related to a

reference impedance measurement previously recorded (usually the reference is the average impedance distribution calculated over the preceding breath cycles). In addition, the EIT device calculates functional EIT image vectors $\mathbf{f}(t_k)$ based on the standard deviation over the preceding breath cycles [4].

After temporal low-pass filtering with a corner frequency of $f_c = 50\ min^{-1}$ to suppress cardiac-related impedance changes, the functional EIT image vector **f** at the beginning of the slow inflation was used to determine the region of interest (ROI, i.e. the lung region) by setting a threshold to 15% of the maximum value of **f**. Therefore, we calculated new image vectors $\Delta\mathbf{z}^*(t_k)$ with $N_L<912$ elements containing only the N_L elements of the lung ROI (using the mask derived from thresholding **f**). For simplicity, we will denominate $\Delta\mathbf{z}^*(t_k)$ as $\Delta\mathbf{z}(t_k)$ from now on. We then discarded all image vectors taken outside the low flow breath retaining N vectors $\Delta\mathbf{z}(t_k)$ with k = 1…N wherein k = 1 designates the beginning and k = N the end of the low flow breath. $t_1 = t_{min}$ and $t_N = t_{max}$ were derived from the minimum and maximum of the global impedance change $\Delta Z(t_k)$ which is given by the sum over all pixels in the lung ROI:

$$\Delta Z(t_k) = \sum_{i=1}^{N_L} \Delta z_i(t_k) \qquad (1)$$

Afterwards, each pixel time curve $\Delta z_i(t_k)$ was normalized to its respective impedance values at times t_{min} and t_{max}:

$$\Delta z_i^{norm}(t_k) = \frac{\Delta z_i(t_k) - \Delta z_i(t_{\min})}{\Delta z_i(t_{\max}) - \Delta z_i(t_{\min})} \cdot 100\% \quad \text{for all} \quad i = 1...N_L, k = 1...N \ . \qquad (2)$$

Figure S1 exemplary shows three different normalized regional curves Δz_i^{norm} from the boundaries (ventral and dorsal) measured in one representative animal.

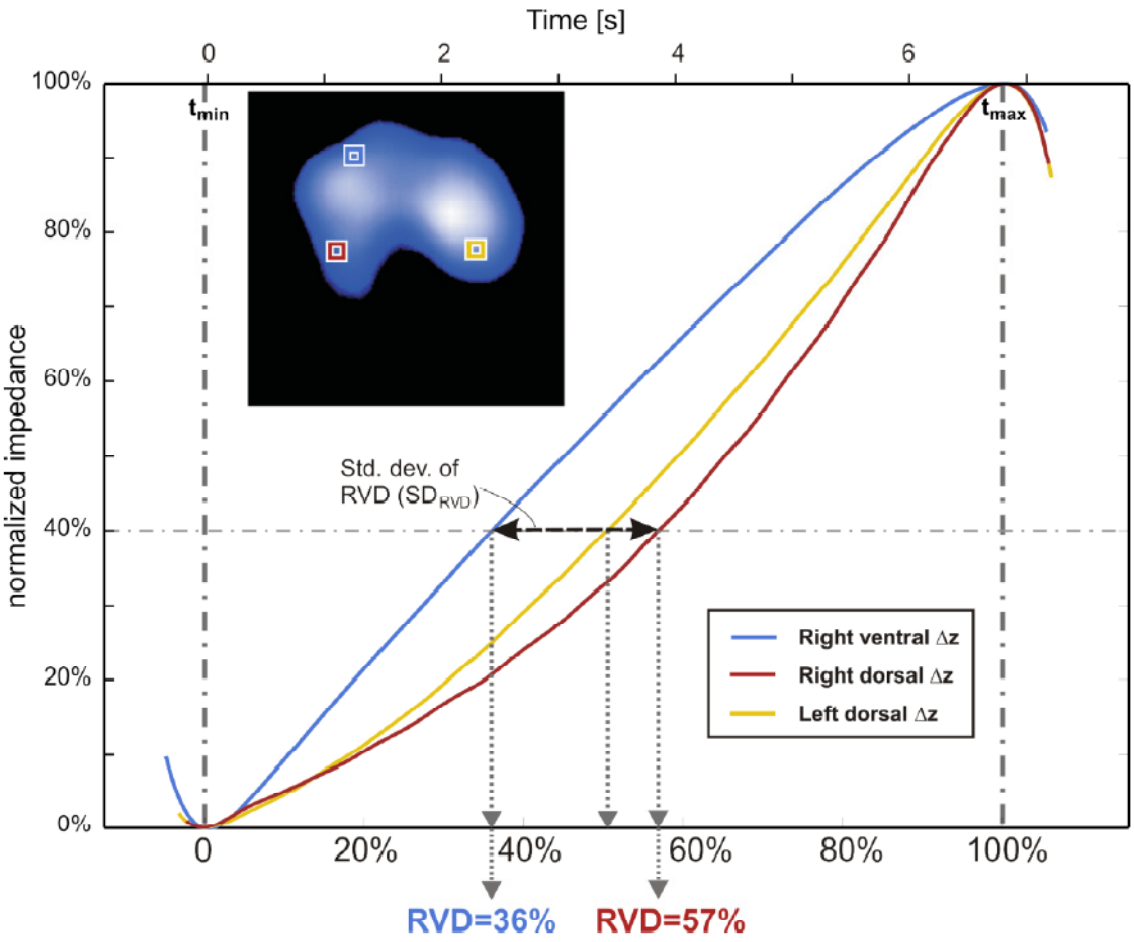

Fig. S1: Normalized regional impedance curves Δznorm during a slow inflation (all curves are normalized to the beginning and end of the low flow breath, see equations 1) and 2).

It can clearly be seen that the aeration of the dorsal regions is delayed due to tidal lung collapse. It takes 57% of the complete maneuver time (t_{max}-t_{min}) for the impedance of the left dorsal region to reach 40% of its maximum value on the ordinate whereas it only takes 36% in the right ventral region. Thus, these percent values are denominated as regional ventilation delay (RVD_i) for each pixel i=1…N_L in the lung region and are computed as

$$RVD_i = \frac{\Delta t_i^{40\%}}{t_{\max} - t_{\min}} \cdot 100\% \qquad (3)$$

where $\Delta t_i^{40\%}$ is the time it takes the normalized impedance of the ith pixel to reach 40% of its maximum value during the slow inflation maneuver. This calculation is a pixel-wise refinement of the quadrant-based regional ventilation delay index described in [3].

The 40% threshold on the ordinate was chosen based on the examination of the data at hand. At this threshold, we found the largest variance of delay times which lead to an improved resolution robustness of the RVD index. For completeness, we additionally tested other thresholds and also used curve-fitting methods, but did not obtain better results (see chapter SDC-3). We decided to stick to the 40%-RVD index due to its computational efficiency and its simplicity.

In this way, we get a pixel-wise regional ventilation delay index which can then be graphically depicted in a color-encoded regional ventilation delay map (RVD map), see figure S2.

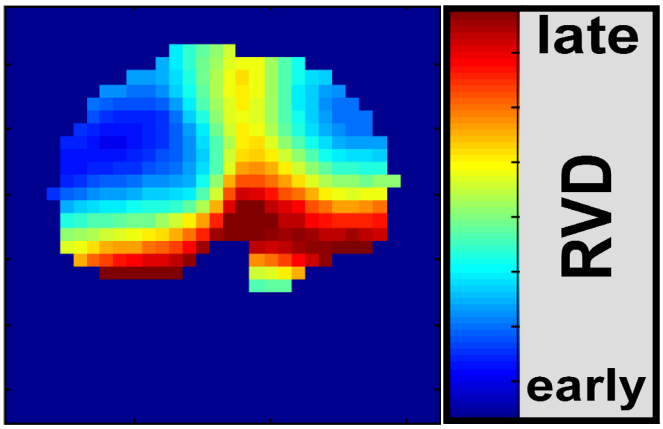

Fig. S2: Regional ventilation delay map depicting the color-encoded distribution of regional ventilation delay times in a diseased pig lung. Red areas have a high delay, i.e. they open comparatively late. The more homogenous the color distribution, the lower SDRVD will become (for SDRVD equal to zero, the whole map would be green).

These maps visualize the regional distribution of delay times which are considerably increased in the dorsal lung regions due to end-tidal lung collapse (provided that we are ventilating diseased pigs with low PEEP). Even though these maps lend themselves

conveniently to fast visual inspection by the attending medical staff, they do not provide a proper quantification of the effect of tidal collapse in form of a scalar parameter. Therefore, we decided to introduce a scalar quantity referred to as SD_{RVD} by computing the standard deviation over all delay indices in the lung region:

$$SD_{RVD} = \sqrt{\frac{\sum_{i=1}^{N_L}\left(RVD_i - RVD_{mean}\right)^2}{N_L - 1}} \qquad \text{with} \qquad RVD_{mean} = \frac{\sum_{i=1}^{N_L} RVD_i}{N_L} \qquad (4)$$

This new index provides a mathematical approximation of the inhomogeneity of regional delay times in the lung. If all parts of the lung were opening at the same time, the index would be zero. The more the opening dynamics vary between different lung regions, the higher the index value will become.

The number of included pixels is varying within a pig, since size of the ventilated (and EIT signal generating lung) is increasing with recruitment and higher lung volumes at different PEEP levels. In principle, changed inhomogeneity could also be numerically caused by simply changing the number of pixels that are included into the calculation. Thus, regional delay inhomogeneity may be affected by changes in lung volume and filtering of noise in the EIT signal. Hence, one could assume that a decrease in inhomogeneity with higher PEEP levels is mainly caused by a rise in EELV. We found EELV to be nonlinearly correlated with SD_{RVD} ($r=0.84$, $p<0.001$), Therefore the strictly linear correlation of tidal recruitment and SD_{RVD} seems not to be a function of EELV and the effect of changes in the number of investigated pixels appears to be limited. We also tested several filtering thresholds and found that thresholds below 15% decreased signal-to-noise ratio and thereby disproved correlation of CT and EIT parameters.

SDC-2 CT data acquisition and processing

A CT scan measures the reduction of x-ray intensity passing through matter with differing densities (or different linear attenuation coefficients to be precise). In the lung region, a good approximation of the relation of gas and tissue volumes can be derived from a measured CT number (given in Hounsfield Units, HU) using the following equation [5]:

$$CT = -1000\,\mathrm{HU} \cdot \frac{\text{volume of gas}}{\text{volume of gas} + \text{volume of tissue}} = -1000\,\mathrm{HU} \cdot \frac{V_{gas}}{V_{gas} + V_{tis}} \,. \qquad (5)$$

Thus, each voxel is split up into two compartments of gas and tissue, so that the voxel volume is

$$V^{vxl} = V^{vxl}_{gas} + V^{vxl}_{tis} \qquad (6)$$

The voxel volume itself is defined by the resolution of the CT scanner and can be calculated as the product of CT scan dependent pixel area and slice thickness.

Hence, we can deduce the gas and tissue volumes of any given lung voxel as

$$V^{vxl}_{gas} = \frac{CT^{vxl}}{-1000\,\mathrm{HU}} \cdot V^{vxl} \qquad (7) \quad \text{and} \quad V^{vxl}_{tis} = \left(1 - \frac{CT^{vxl}}{-1000\,\mathrm{HU}}\right) \cdot V^{vxl} \qquad (8)$$

Assuming a tissue density close to the density of water (≈ 1 g/ml), the tissue volume in ml can alternatively be interpreted as tissue weight in gram. Equations (7) and (8) are only valid for 0 HU ≥ CT^{vxl} ≥ -1000 HU. If the measured density is higher than the density of water (CT^{vxl} > 0 HU), the voxel is assumed to contain no gas at all, so that

$V^{vxl} = V^{vxl}_{tis}$ and $V^{vxl}_{gas} = 0\,\mathrm{ml}$.

We can now derive important respiratory parameters such as functional residual capacity (FRC) or lung volume V_{lung}. FRC is computed as

$$FRC = \sum_{\text{all lung voxels}} V^{vxl}_{gas} \qquad (9)$$

which is the sum over all gas volumes of all lung voxels having CT values between 0 HU and -1000 HU.

The lung volume is given as

$$V_{lung} = \sum_{\text{all lung voxels}} V^{vxl} = N_{\text{lung}} \cdot V^{vxl} \qquad (10)$$

where N_{lung} is the number of lung voxels of the whole lung and V^{vxl} is the constant voxel volume.

During our study, we defined the lung regions manually in each CT slice as regions of interest excluding mediastinal organs. We used a CT scan analysis software named Osiris (from the University of Geneva, Switzerland) and manually discriminated between the right and the left lobe of the lung. Equivalent quadrants were separated considering the whole transversal slice (including extrapulmonary tissue surrounded by EIT electrodes).

To further distinguish between different degrees of aeration, it is possible to set certain CT thresholds which can be found in the literature [5]:

- **non-aerated lung tissue** with (+100 HU ≥) 0 HU ≥ CT > -100 HU
- **poorly-aerated lung tissue** with -100 HU ≥ CT > -500 HU
- **normally-aerated lung tissue** with -500 HU ≥ CT > -900 HU
- **hyper-inflated lung tissue** with -900 HU ≥ CT > -1000 HU

As we were aiming at measuring tidal recruitment, we looked at the volume of non-aerated lung tissue (+100 HU ≥ CT > -100 HU) at the end of inspiration and expiration. The respective volumes were computed following the considerations leading to equation (10) using CT scans at the end of an inspiration and a subsequent expiration:

$$V_{\text{non-aerated lung, insp}} = N_{\text{non-aerated lung, insp}} \cdot V^{vxl} \qquad (11)$$

$$V_{\text{non-aerated lung, exp}} = N_{\text{non-aerated lung, exp}} \cdot V^{vxl} \qquad (12)$$

where $N_{\text{non-aerated lung, insp}}$ ($N_{\text{non-aerated lung, exp}}$) is the number of voxels containing non-aerated lung at the end of inspiration (expiration).

We then defined the percentage of tidal recruitment as

$$\text{perc. tidal recruitment} = \frac{V_{\text{non-aerated lung, exp}} - V_{\text{non-aerated lung, insp}}}{V_{\text{lung}}} \qquad (13)$$

Currently, a scientific debate concentrates on the possible underlying mechanisms of tidal recruitment such as cyclic opening and closing of collapsed alveoli or the movement of air and foam in liquid filled space, which goes far beyond the scope of this paper. This issue we have intensively discussed previously [8]. However, the densitometric CT analysis presented here certainly reflects tidal changes in gas and/or fluid content of the lung tissue during ventilation. Without doubt, these processes on the alveolar scale will lead to the development of ventilator induced lung injury and, regardless of the mechanisms involved to impaired patient outcome. Consequently, the quantification of tidal recruitment by EIT at the bedside may help to individualize ventilator management.

In addition to tidal recruitment, alveolar hyperdistention is supposed to cause ventilator associated lung injury. Unfortunately, the use of CT to detect hyperdistention is questionable since it has clearly been shown that the amount of lung tissue identified as "hyperinflated" significantly depends on the selected reconstruction filter [9].

SDC-3 Gas exchange, respiratory and hemodynamic parameters

Detailed tables on cardio-respiratory and gas exchange parameters are given in tables S1, S2 and S3. Three hours after induction of ALI, animals had severe oxygenation failure. Oxygenation, that was significantly higher in the control group when compared to ALI pigs ($p < 0.05$), increased significantly with higher PEEP levels ($p < 0.001$) independent from lung injury (figure S3 C). Likewise, venous admixture, that was notably higher in the ALI group ($p < 0.05$), decreased, whenever PEEP was increased ($p < 0.001$). This effect was more pronounced in the ALI group ($p < 0.05$ for interaction of factors "group" and PEEP"). Whereas arterial CO_2 was comparable between groups and at all PEEP levels, end tidal CO_2, that was lower in lung injured pigs ($p < 0.05$), increased with higher PEEP levels ($p < 0.001$). Minute ventilation was higher in healthy control pigs ($p < 0.05$) since body weight of these animals was minimal but significant higher. Tidal volume was constant over time and comparable between both groups when normalized to body weight. Whereas compliance of the respiratory system increased in lung injured animals, whenever PEEP was increased ($p < 0.001$), compliance of healthy animals showed a different pattern and started to decrease again with highest PEEP levels ($p < 0.001$ for interaction of factors "group" and PEEP", figure S3 A).

The amount of non aerated lung tissue at PEEP 0 in control pigs was almost negligible and decreased slightly to 1 ± 1 % at PEEP of 10 cm H2O. However, in these animals, compliance of the respiratory system increased by 67% between PEEP 0 and 10, while PaO_2/FiO_2 increased by 40%, suggesting significant alveolar recruitment by PEEP. Furthermore, Qs/Qt was relatively high at PEEP 0 (15 ± 3%) in normal animals, suggesting occurrence of atelectasis related to anesthesia. In healthy pigs the amount of poorly aerated lung tissue (-100 to -500 HU) was reduced from 40% at zero PEEP to less than 10% with

increasing PEEP. This might explain improvement of oxygenation since also poorly aerated lung tissue (low Va/Q areas) may contribute to venouse admixture.

The plateau pressures we reached (table S2) in our animals were higher than clinically usual, especially at high PEEP levels. In our lung injury model we used an intraabdominal pressure of 20 cm H2O to ensure pronounced and repeatedly producible lung derecruitment, what was essential when validating our method. This, certainly, caused a massive reduction in chest wall compliance. Thus, the increase in transpulmonary pressures should be limited even when plateau pressures were high.

Increasing PEEP levels led to a decrease in cardiac output and mean arterial blood pressure ($p < 0.001$, respectively). Hemodynamic depression and increase in heart rate was more pronounced in control pigs ($p < 0.001$ interaction of factors “group” and PEEP”, respectively), that showed a significant decrease in intrathoracic blood volume and stroke volume at higher PEEP steps ($p < 0.001$ interaction of factors “group” and PEEP”, respectively).

Table S1 – hemodynamic parameters

mean ± SD		PEEP in [cm H_2O]						ANOVA		
Parameter	Group	0	5	10	15	20	25	PEEP	Group	Interaction
MAP	control	132 ± 23	118 ± 14	110 ± 22	74 ± 19	84 ± 27	76 ± 13	a	n.s.	a
[mmHg]	ALI	113 ± 22	115 ± 22	114 ± 17	111 ± 21	128 ± 21	122 ± 19			
CO	control	4.3 ± 0.5	3.7 ± 0.5	3.0 ± 0.3	2.6 ± 0.4	2.4 ± 0.4	1.8 ± 0.4	a	b	a
[1/min]	ALI	4.7 ± 1.1	4.8 ± 1.1	4.6 ± 1.1	4.1 ± 0.9	4.5 ± 1.2	3.9 ± 1.1			
HR	control	105 ± 12	107 ± 21	99 ± 17	118 ± 23	117 ± 18	112 ± 20	n.s.	b	b
[1/min]	ALI	90 ± 8	93 ± 3	89 ± 9	86 ± 8	88 ± 7	89 ± 12			
EVLW	controll	391 ± 47	352 ± 66	359 ± 60	344 ± 36	334 ± 31	280 ± 39	n.s.	n.s.	n.s.
[ml]	ALI	476 ± 129	476 ± 122	455 ± 89	498 ± 236	508 ± 234	457 ± 195			
ITBV	control	506 ± 47	473 ± 49	540 ± 83	377 ± 48	371 ± 52	357 ± 37	a	b	b
[ml]	ALI	531 ± 110	536 ± 106	450 ± 46	534 ± 82	571 ± 140	499 ± 81			
SV	control	37 ± 6	32 ± 8	29 ± 3	22 ± 7	20 ± 3	13 ± 5	a	a	b
[ml]	ALI	50 ± 8	50 ± 11	50 ± 11	47 ± 7	53 ± 14	42 ± 13			
SVV	control	14 ± 4	13 ± 8	9 ± 3	16 ± 4	19 ± 4	17 ± 6	n.s.	b	b
[%]	ALI	10 ± 3	9 ± 4	12 ± 5	10 ± 2	10 ± 4	11 ± 2			
CVP	control	10 ± 2	11 ± 2	14 ± 2	15 ± 1	17 ± 5	16 ± 1	a	n.s.	n.s.
[mmHg]	ALI	14 ± 3	16 ± 3	16 ± 4	17 ± 3	20 ± 5	22 ± 7			
MPAP	control	48 ± 4	33 ± 11	31 ± 11	35 ± 11	36 ± 8	36 ± 7	n.s.	n.s.	b
[mmHg]	ALI	44 ± 9	43 ± 10	44 ± 10	38 ± 9	41 ± 6	42± 6			

Mean arterial blood pressure (MAP), cardiac output (CO), heart rate (HR), extra vascular lung water (EVLW), intra thoracal blood volume (ITBV), stroke volume (SV), stroke volume variation (SVV), central venous blood pressure (CVP) and mean pulmonary artery blood pressure (MPAP) for healthy (control) and lung injured (ALI) pigs with changes in PEEP from zero to 25 cm H_2O. Data are given as means and SD.

Repeated measures ANOVA: [a] $p < 0.001$ and [b] $p < 0.05$ for factors *PEEP*, *Group* and *interaction of PEEP and Group,* respectively.

Table S2 – respiratory parameters

mean ± SD		PEEP in [cm H_2O]						ANOVA		
Parameter	Group	0	5	10	15	20	25	PEEP	Group	Interaction
V_T/kg BW	control	7.8 ± 0.2	7.5 ± 0.2	7.4 ± 0.3	7.6 ± 0.2	7.5 ± 0.2	7.6 ± 0.5	n.s.	n.s.	n.s.
[ml/kg BW]	ALI	7.8 ± 0.4	7.9 ± 0.2	7.8 ± 0.3	7.8 ± 0.3	7.7 ± 0.3	7.9 ± 0.4			
MV	control	6.2 ± 0.9	5.8 ± 0.8	5.8 ± 0.7	5.9 ± 0.9	5.7 ± 0.9	5.8 ± 0.8	n.s.	b	n.s.
[l/min]	ALI	5.6 ± 0.9	5.6 ± 1.1	5.2 ± 0.3	5.4 ± 1.4	5.4 ± 1.3	5.4 ± 1.2			
C	control	16 ± 2	22 ± 6	27 ± 7	26 ± 9	22 ± 5	14 ± 1	a	a	a
[ml/cmH_2O]	ALI	5 ± 1	7 ± 1	7 ± 1	10 ± 4	11 ± 2	9 ± 2			
R	control	12 ± 1	17 ± 2	10 ± 1	10 ± 2	10 ± 2	11 ± 4	a	a	a
[kPa/l/s]	ALI	30 ± 7	27 ± 5	25 ± 5	20 ± 7	20 ± 3	21 ± 3			
$P_{aw.mean}$	control	7 ± 1	9 ± 1	13 ± 1	19 ± 1	24 ± 1	31 ± 1	a	a	a
[cmH_2O]	ALI	15 ± 3	16 ± 4	19 ± 2	21 ± 2	26 ± 1	32 ± 1			
$P_{aw.plat}$	control	16 ± 3	16 ± 4	18 ± 2	24 ± 4	31 ± 4	42 ± 2	a	a	a
[cmH_2O]	ALI	40 ± 8	38 ± 8	39 ± 6	36 ± 7	40 ± 5	48 ± 4			
$P_{aw.peak}$	control	18 ± 3	18 ± 4	20 ± 2	26 ± 4	33 ± 4	44 ± 2	a	a	a
[cmH_2O]	ALI	42 ± 8	40 ± 8	41 ± 6	38 ± 7	42 ± 5	49 ± 4			
RR	control	23 ± 3	23 ± 3	23 ± 3	23 ± 3	23 ± 3	23 ± 3	n.s.	n.s.	n.s.
[1/min]	ALI	25 ± 4	25 ± 4	24 ± 4	24 ± 4	24 ± 4	24 ± 4			

Tidal volume per kilogram of body weight (VT/kg BW), minute ventilation (MV), global respiratory compliance (C), resistance (R), mean airway pressure (Paw.mean), peak airway pressure (Paw.peak) and respiratory rate (RR) for healthy (control) and lung injured (ALI) pigs with changes in PEEP from zero to 25 cm H_2O. Data are given as means and SD. Repeated measures ANOVA: [a] $p < 0.001$ and [b] $p < 0.05$ for factors *PEEP*, *Group* and *interaction of PEEP and Group,* respectively.

Table S3 – gas exchange parameters

mean ± SD		PEEP in [cm H_2O]						ANOVA		
Parameter	Group	0	5	10	15	20	25	PEEP	Group	Interaction
PaO_2/F_iO_2	control	252 ± 29	324 ± 71	353 ± 145	388 ± 137	475 ± 74	499 ± 50	a	b	n.s.
[torr]	ALI	98 ± 66	105 ± 100	168 ± 151	236 ± 138	353 ± 122	405 ± 199			
SaO_2	control	98 ± 1	99 ± 1	97 ± 6	99 ± 1	99 ± 1	99 ± 1	b	p=0.067	b
[%]	ALI	83 ± 18	85 ± 14	90 ± 10	96 ± 6	99 ± 1	99 ± 4			
$PaCO_2$	control	47 ± 10	45 ± 11	47 ± 14	49 ± 10	48 ± 10	46 ± 10	n.s.	n.s.	n.s.
[torr]	ALI	45 ± 10	43 ± 10	38 ± 7	39 ± 6	37 ± 5	37 ± 5			
$etCO_2$	control	34 ± 12	35 ± 12	35 ± 5	40 ± 10	41 ± 9	39 ± 8	a	b	n.s.
[torr]	ALI	23 ± 4	24 ± 4	26 ± 4	28 ± 4	29 ± 4	30 ± 3			
Qs/Qt	control	15 ± 3	10 ± 3	11 ± 1	4 ± 3	3 ± 2	2 ± 1	a	b	b
[%]	ALI	44 ± 21	43 ± 19	32 ± 17	21 ± 13	12 ± 5	11 ± 10			
DO_2	control	828 ± 95	777 ± 121	618 ± 105	550 ± 94	532 ± 84	414 ± 100	b	n.s.	a
[ml/min]	ALI	663 ± 195	682 ± 169	669 ± 131	708 ± 152	821 ± 129	797 ± 191			

Oxygenation (PaO_2/F_iO_2), arterial oxygen saturation (SaO_2), arterial carbon dioxide tension ($PaCO_2$), end-tidal carbon dioxide tension ($etCO_2$), pulmonary venous admixture (Qs/Qt) and oxygen delivery (DO_2) for healthy (control) and lung injured (ALI) pigs with changes in PEEP from zero to 25 cm H_2O. Data are given as means and SD.

Repeated measures ANOVA: [a] $p < 0.001$ and [b] $p < 0.05$ for factors *PEEP*, *Group* and *interaction of PEEP and Group,* respectively.

Global respiratory compliance was influenced by severity of lung injury *per se*, since it was found to be always higher in healthy pigs (SDC table S2 and figure S3A). A massive reduction in chest wall compliance in our model of lung injury due to intra-abdominal hypertension may have aggravated this matter.

Tidal recruitment can increase venous admixture and may thereby affect oxygenation. In this study, arterial oxygenation – not surprisingly - was not helpful to detect changes in tidal recruitment since arterial oxygenation is influenced by pulmonary and extrapulmonary factors, such as EELV and oxygen delivery/demand balance. However, oxygenation and tidal recruitment showed a significant correlation. Since a derecruited lung is prone to tidal recruitment whereas a recruited lung is not there is an indirect link what might explain this finding.

Compliance and PaO_2/FiO_2 were correlated with tidal recruitment rather non-linearly than linearly (figure S3). Referring to Spearman's rank difference correlation coefficients, SD_{RVD} showed the strongest correlation with tidal recruitment when calculated for ALI (ρ = 0.84) group and all animals (ρ = 0.77).

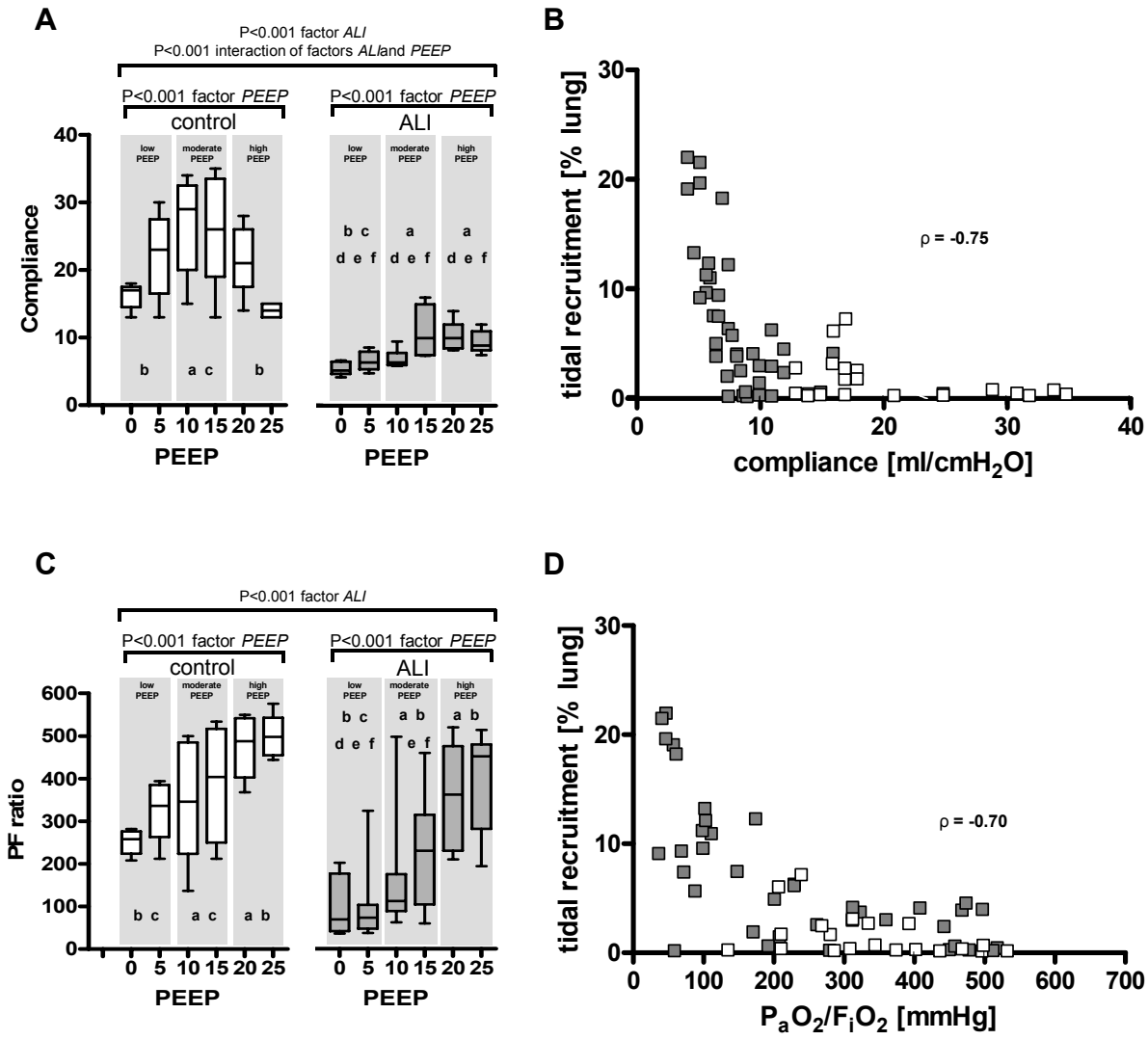

Fig. S3: A: course of global compliance of the respiratory system (CRS) with changes in positive end-expiratory pressure (PEEP) from zero to 25 cmH_2O in healthy (control: outlined boxes) and lung-injured (ALI, filled boxes) pigs. B: linear correlation between amount of tidal recruitment in % of lung and CRS. Outlined boxes: control pigs, filled boxes: ALI pigs. ρ = Spearman´s rank difference correlation coefficient. C: course of global oxygenation (P_aO_2/F_iO_2) with changes in positive end-expiratory pressure (PEEP) from zero to 25 cmH_2O in healthy (control. outlined boxes) and lung-injured (ALI, filled boxes) pigs. D: linear correlation between amount of tidal

recruitment in % of lung and P_aO_2/F_iO_2. Outlined boxes: control pigs, filled boxes: ALI pigs. ρ = Spearman´s rank difference correlation coefficient.

Statistics: repeated measures ANOVA with factors "*ALI*" (for differences between healthy and lung-injured animals) and *"PEEP"* (for differences between PEEP levels). Post hoc tests (Newman-Keuls-test) to separate differences between low (0 and 5 cmH_2O), moderate (10 and 15 cmH_2O) and high (20 and 25 cmH_2O) PEEP within one group (a: $p < 0.05$ vs. low PEEP, b: $p < 0.05$ vs. middle PEEP, c: $p < 0.05$ vs. high PEEP) and between both groups (d: $p < 0.05$ vs. control low PEEP, e: $p < 0.05$ vs. control middle PEEP, f: $p < 0.05$ vs. control high PEEP). Box plots show median and quartiles.

SDC 4 regular breath vs. slow inflation maneuver for SD_{RVD} calculation

The question arises why EIT analyzes were not performed during a regular breath but during a slow inflation with a lightly increased tidal volume.

We also calculated SD_{RVD} from EIT signals recorded from normal tidal volumes that were applied preceding the slow inflation maneuvers were performed. Data are shown in figure S4.

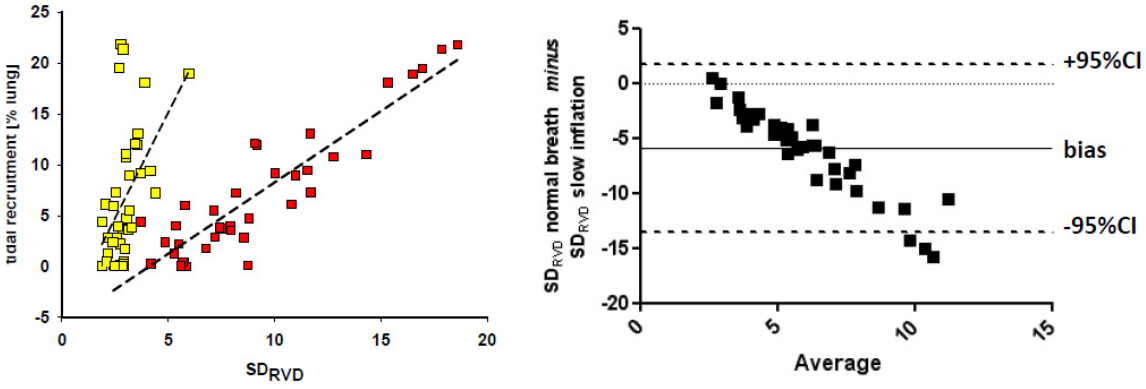

Fig. S4: left: linear correlation between tidal recruitment (measured by CT during a normal breath) and SD_{RVD} calculated from normal 8 ml/kg breath (yellow squares, r=0.48, p<0.01) and linear correlation between tidal recruitment and SD_{RVD} calculated from the 12 ml/kg slow inflation maneuver (red squares, r=0.92, p<0.001); right: Bland-and-Altmann comparison between SD_{RVD} calculated from normal 8 ml/kg breath and SD_{RVD} calculated from the 12 ml/kg slow inflation maneuver.

Whereas the slow inflation-SD_{RVD} were excellently correlating with tidal recruitment and discriminable between different PEEP levels, normal-breath-SD_{RVD} were not. Bland-and-Altmann comparison of both parameters showed that normal-breath-SD_{RVD} always underestimated Regional-Ventilation-Ddelay-Inhomogeneity when compared to slow–inflation-SD_{RVD}. This effect was more pronounced the higher tidal recruitment (and hence, the lower the PEEP level) was. This suggests that calculation of Regional-Ventilation-Ddelay-Inhomogeneity requires a slow inflation of a lightly increased tidal volume.

The following methodological consideration might explain why SD_{RVD} calculated from a normal breath did not lead to valid information on tidal recruitment. The basic principle of our

method is quantifying inhomogeneity of regional ventilation time courses. A schematic depiction of a bundle of normalized regional impedance- (or volume-) time curves is displayed in figure S5.

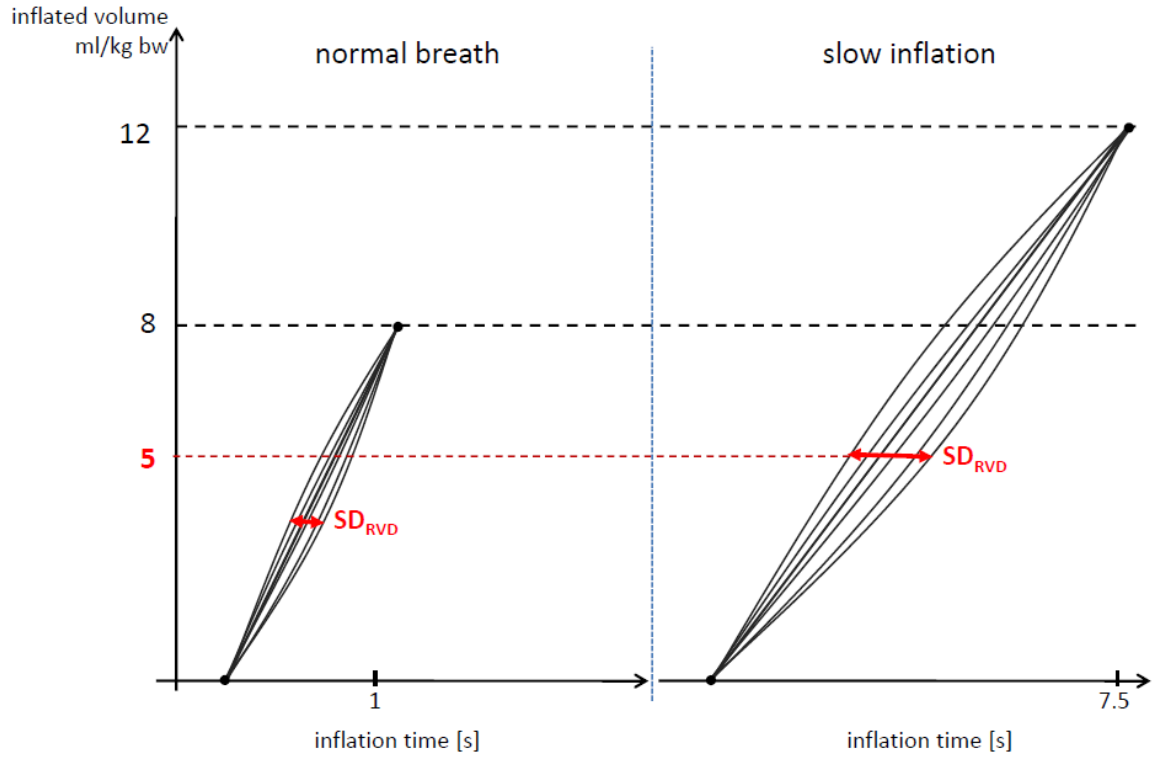

Fig. S5: schematic depiction of normalized regional impedance- (or volume-) time curves during inflation of a normal breath of 8 ml/gk BW (left picture) and during a 12ml/kg BW slow inflation maneuver (right picture). Regional delay inhomogeneity (SDRVD) is displayed as a red bidirectional arrow and quantifies the "spindle-like" splitting of the bundle.

Based on regionally different machanical conditions on a certain PEEP level different ventilatory units of the lung show different time courses of filling during a normal breath (fig S5, left part). Thus, when normalized to 100 % of the regional maximal filling, regional curves show a "spindle-like" splitting. SD_{RVD} quantifies the extent of this splitting. The larger SD_{RVD} (the longer the bidirectional arrow in figure S5) the higher the inhomogeneity in regional filling characteristics is. When a respiratory rate of 30/min (as done in our experiments) with an I:E ratio of 1 is applied, inflation time is 1 s. As we sampled EIT

tracings with a frequency of 20 Hz 20 data points were available to measure inhomogeneity of up to 912 regional impedance-time curves what results in a low signal-to-noise-ratio. This explains why calculating SD_{RVD} from a normal breath with a regular tidal volume of 8 ml/kg did not lead to valid results in our experimental setting. In contrast, based on the identical mechanical conditions at the same PEEP level SD_{RVD} is increased by simply both stretching inflation time and lightly increasing inflation volume during a 12 ml/kg BW slow inflation maneuver. This effect is illustrated by an elongated arrow in figure S5 (right part, note that, additionally, time scale is compressed in the right figure). Thus, signal-to-noise ratio and sensibility of this measure is improved and the signal to be quantified is somehow "adapted" to the temporal resolution of the measurement technique.

Further, it is mentionable that the inflated volume at time point of pixelwise RVD-quantification (40% of the local maximum) is around 5 ml/kg BW and, thus within the range of a regular tidal volume. This considerations strongly suggest that, although obtained during an artificial maneuver with different flow and inflation volume, measurement of SD_{RVD} delineates inhomogeneity in regional lung mechanics at a certain PEEP level that in turn are affecting tidal recruitment.

SDC-5 Curve fitting for index validation

To test the feasibility of using the much simpler and computationally more efficient 40% threshold approach instead of more refined curve fitting algorithms, we fitted the following three different model curves $f_m(t;\beta)$ in a Least Squares (LS) sense to our impedance time curves and compared the resulting fitting parameters $\beta = (a,b,c)^T$ with SD_{RVD} regarding their ability to quantify tidal recruitment:

$$f_{m1}(t;a,b,c) = a \cdot t^b + \mathrm{c} \qquad (14)$$

$$f_{m2}(t;a,b,c) = a \cdot (t-c)^b \qquad (15)$$

$$f_{m3}(t;a,b,c) = \frac{a}{1+e^{-(t-b)/c}} \qquad (16)$$

The LS curve fitting problem to be solved is stated as follows: given a discrete set of empirical pairs of independent and dependent variables $[t_k, \Delta z^{norm}(t_k)]$, we need to optimize the parameters β of the presented model curves $f_m(t;\beta)$ so that the sum of the squares of the deviations

$$S(\beta) = \sum_{k=1}^{N} [\Delta z^{norm}(t_k) - f_m(t_k;\beta)]^2 \qquad (17)$$

becomes minimal. To solve this problem, we used the pixel-wise applied iterative curve-fitting algorithm of Levenberg and Marquardt provided by a customized MATLAB-software (MATLAB 7.5, The MathWorks, Inc., USA) [6,7]. Correlation coefficients (r between several fitting parameters and tidal recruitment and r for correlation between the 40% as well as a 10% threshold and tidal recruitment are shown in table S4.

Table S4

Correlation Coefficients r

tidal recruitment vs.

	Thresholds		Curve Fitting								
	40%	10%	f_{m1}			f_{m2}			f_{m3}		
			a	*b*	*c*	*a*	*b*	*c*	*a*	*B*	*c*
All pigs	0.91	0.90	0.72	0.88	0.66	0.75	0.90	0.71	0.52	0.79	0.77
Pig 1	0.98	0.99	0.99	0.99	0.97	0.97	0.98	0.83	0.10	0.92	0.96
Pig 2	0.90	0.92	0.64	0.36	0.65	0.93	0.92	0.96	0.93	0.91	0.65
Pig 3	0.98	0.96	0.93	0.96	0.91	0.577	0.94	0.82	0.73	0.87	0.82
Pig 4	0.98	0.95	0.40	0.99	0.42	0.99	0.99	0.98	0.98	0.97	0.85
Pig 5	0.97	0.89	0.45	0.77	0.10	0.0,51	0.94	0.0,26	0.28	0.95	0.10
Pig 6	0.96	0.96	0.42	0.88	0.52	0.86	0.92	0.77	0.85	0.93	0.94
Pig 7	0.95	0.94	0.24	0.94	0.57	0.82	0.94	0.75	0.91	0.92	0.71

The best fitting parameter is *b* of model curve f_{m2} (light grey). It shows comparable performance with the used 40% threshold parameter (RVD. dark grey), but the computational burden is much higher.

SDC-6 Selection of lung injury model

Even though the oleic acid injection model of lung injury is widely used, as this model mimics the pathological features of ARDS, comparisons with patients suffering from ALI or ARDS should be drawn with caution. In patients with a more focal loss of lung aeration and low potential for alveolar recruitment regional mechanical characteristics may differ from that in our model. The question arises, if a further group of animals with a direct model of ALI would expand our results. In a previous investigation [3], we inflated 1200 ml (lung capacity slow inflation maneuver) during dynamic CT scan with a temporal resolution of 10 Hz, meaning that a new CT image of the respective slice was performed every 100 ms. Thus, we were able to analyze recruitment at different time points of the 1200 ml inflation and,

therefore, at different inflation volumes. We then displayed recruitment over time and identified the images representing lung tissue at inflation of 400 ml what was around 12 ml/kg (comparable to the inflation used in the present study).

Figure S6 shows that recruitment in the healthy control groups of both studies was comparable, when matched for comparable inflation volumes.

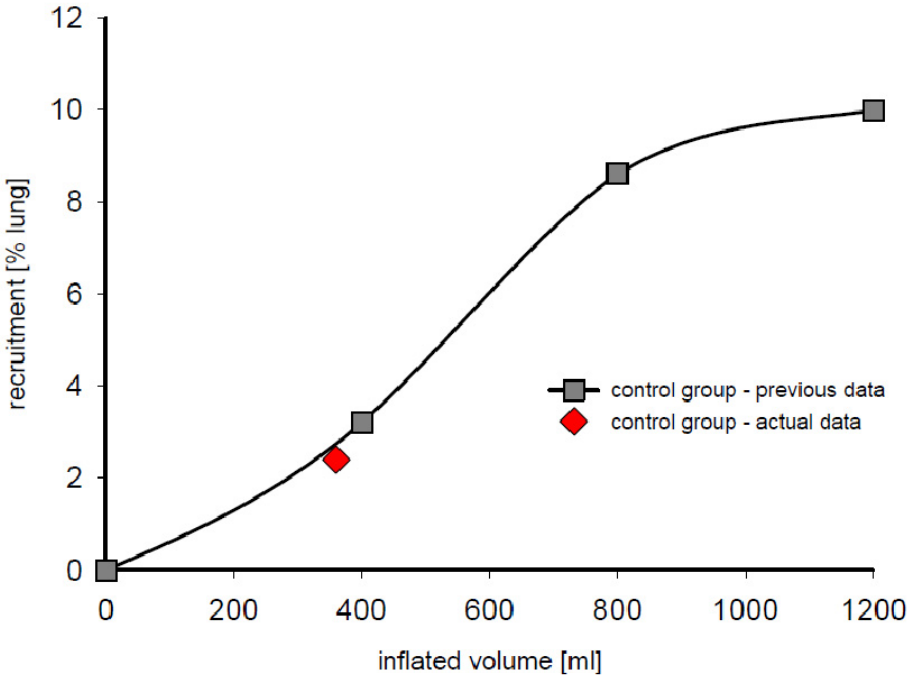

Fig. S6: grey: reanalysis of previously published data [3], recruited lung volume in [% lung] during slow inflation of 1200 ml in healthy pigs; red: recruitment in healthy control pigs of the current study during a 12 ml/kg BW slow inflation.

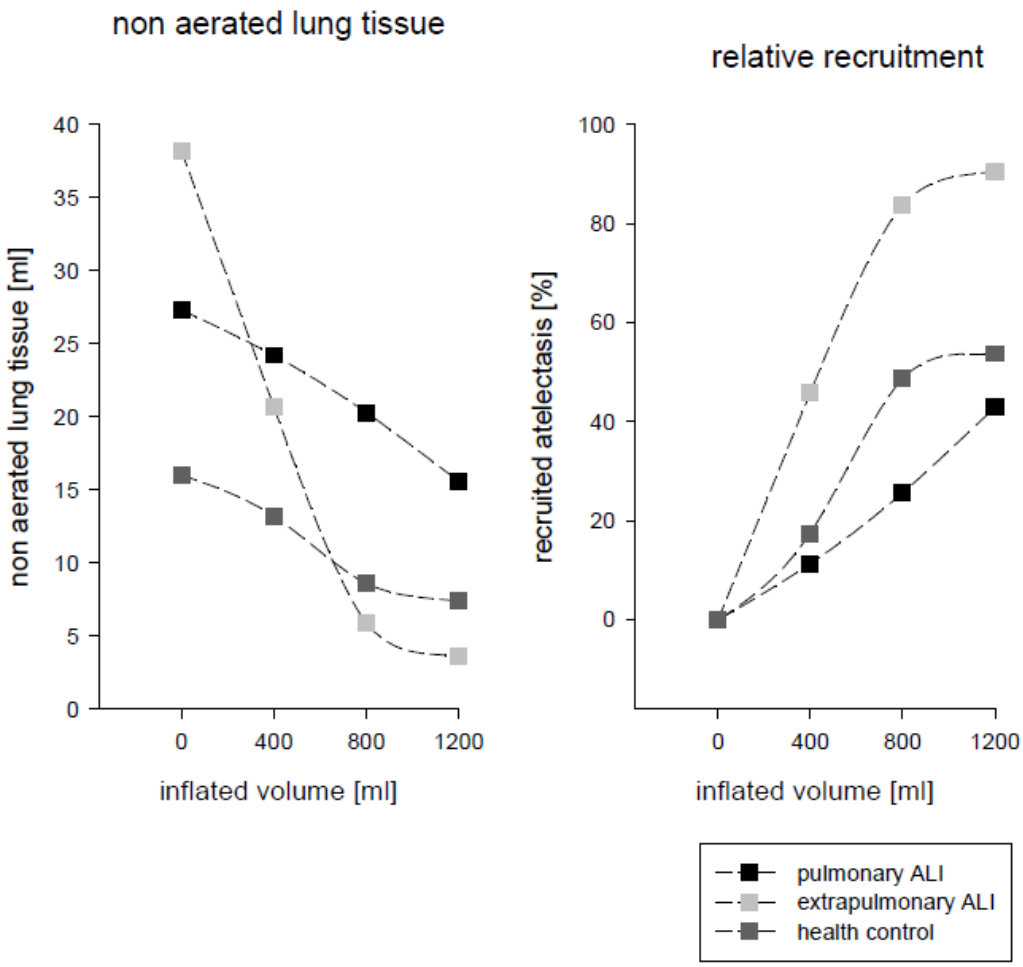

Fig. S7: reanalysis of previously published data [3], non aerated lung tissue (left) and relative recruitment (right) during a 1200 ml slow inflation in pulmonary (direct) ALI, extrapulmonary (indirect) ALI and in healthy pigs.

Figure S7 demonstrates that in our previous experiments pulmonary (direct) ALI and healthy animals showed similar behavior regarding recruitment, especially at lower inflation volumes. Even though the amount of non aerated lung tissue was clearly higher in pulmonary ALI group when compared to control animals (left image), relative recruitment (right image) was lower in pulmonary ALI, indicating that there was some "consolidated" and non recruitable lung tissue. Hence, in our recent experimental setting (12 ml/kg inflation) recruited lung volume in a pulmonary ALI group would not differ (or even underrun) the amount of

tidal recruitment that was observed in our recent control group. Further, the non recruitable atelectasis would not be ventilated and, thus, would not generate an EIT signal. Therefore, it would not be included into the RVD (and SD_{RVD}) analyzes. Finally, for validation purpose groups with a high and a low potential for recruitment are necessary. A further group with low potential for recruitment would not have increased reliability of the present study.

Further, a direct ALI group would be unfeasible for our study for a second reason: we applied different PEEP levels in a randomized order. In between we performed repeated derecruitement and recruitment maneuvers to ensure interindividual comparability. Regarding this issue, the used ALI model provides optimal conditions since it is repeatedly derecruitable due to the increased intraabdominal pressure, whereas a acid aspiration model is not.

Literature

[1] Wrigge H, Zinserling J, Neumann P, Muders T, Magnusson A, Putensen C, Hedenstierna G. Spontaneous breathing with airway pressure release ventilation favors ventilation in dependent lung regions and counters cyclic alveolar collapse in oleic-acid-induced lung injury: a randomized controlled computed tomography trial. Crit Care 2005; 9: R780-R789

[2] Varelmann D, Muders T, Zinserling J, Guenther U, Magnusson A, Hedenstierna G, Putensen C, Wrigge H. Cardiorespiratory effects of spontaneous breathing in two different models of experimental lung injury: a randomized controlled trial. Crit Care 2008; 12: R135

[3] Wrigge H. Zinserling J. Muders T. Varelmann D. Günther U. von der Groeben C. Magnusson A. Hedenstierna G. Putensen C. Electrical impedance tomography compared with thoracic computed tomography during a slow inflation maneuver in experimental models of lung injury. Crit Care Med 2008;36(3):903-9.

[4] Luepschen H. Meier T. Grossherr M. Leibecke T. Karsten J. Leonhardt S. Protective ventilation using electrical impedance tomography. Physiol Meas 2007; 28(7):S247-60.

[5] Gattinoni L. Caironi P. Pelosi P. Goodman LR. What has computed tomography taught us about the acute respiratory distress syndrome? Am J Respir Crit Care Med 2001;164:1701-11.

[6] Levenberg. K. A Method for the Solution of Certain Non-Linear Problems in Least Squares. The Quarterly of Applied Mathematics 1944; 2: 164–168.

[7] Marquardt. M. An Algorithm for Least-Squares Estimation of Nonlinear Parameters. SIAM Journal on Applied Mathematics 1963; 11: 431–441.

[8] Muders T and Wrigge H: New insights into experimental evidence on atelectasis and causes of lung injury. Best Practice and Research Clinical Anaesthesiology 2010; 24: 171-182.

[9] Reske AW, Busse H, Amato MB, et al: Image reconstruction affects computer tomographic assessment of lung hyperinflation. Intensive Care Med 2008; 34: 2044-2053.